PHOTONIC SENSORS / Vol. 4, No. 1, 2014: 86–91

A Method for Eliminating the Impact of Microwave Sweeper Power Fluctuation in BOTDA System

Shuo JIANG, Jun CHANG*, Sasa ZHANG, Zongliang WANG, Sha LUO, Boning SUN, Xiaohui LIU, Yongning LIU, Junqiang TIAN, and Chuanwu JIA

School of Information Science and Engineering and Shandong Provincial Key Laboratory of Laser Technology and Application, Shandong University, Jinan, 250199, P. R. China

*Corresponding author: Jun CHANG E- mail: changjun@sdu.edu.cn

Abstract: The impact of microwave sweeper power fluctuation in the BOTDA system has been theoretically analyzed and experimentally tested. And a novel method comparing real-time acquisition of probe wave power with a new algorithm to realize probe wave power normalization for eliminating this impact was proposed. The principle of the proposed method was described theoretically. And the contrast test between our new method and conventional one was carried out. The experiment results indicated that the temperature accuracy was effectively improved from ±5℃ to ±2℃.

Keywords: Distributed temperature sensor, microwave sweeper power fluctuation, temperature accuracy

Citation: Shuo JIANG, Jun CHANG, Sasa ZHANG, Zongliang WANG, Sha LUO, Boning SUN, *et al*., "A Method for Eliminating the Impact of Microwave Sweeper Power Fluctuation in BOTDA System," *Photonic Sensors*, 2014, 4(1): 86–91.

1. Introduction

The technique of Brillouin optical time domain analysis (BOTDA) distributed optical fiber sensor has been presented and demonstrated experimentally [1, 2]. It has been the main research topic in the past few years owing to the well-known advantages of the optical fiber and its great potential for the engineering applications [3–5].

In the BOTDA system, a pulsed pump beam and a counter-propagating Stokes continuous-wave (CW) probe beam, at different frequencies, are launched into the sensing fiber to generate the stimulated Brillouin scattering (SBS), and the CW probe light is detected [6]. The frequency of the pulse wave after acousto-optic modulation (AOM) is $\nu + \nu_a$ (ν_a is the Doppler frequency shift of the AOM). The CW wave is modulated by an electro-optic modulator (EOM) which is driven by a microwave sweeper. The modulated down-shifted sideband is chosen as the CW probe wave, whose frequency is $\nu + \nu_b$ (ν_b is the frequency of the microwave source). When the frequency difference between these two light waves is equal to the Brillouin frequency shift at that point, there is a maximum energy transfer from the pulse to the CW [7, 8]. The temperature and strain information can be extracted through scanning the Brillouin gain spectrum (BGS).

In the BOTDA system, the frequency of the microwave sweeper is swept from 10.5 GHz to 11.5 GHz, which is scanned across the BGS. The frequency corresponding to the peak value in the BGS is where the Brillouin frequency shift occurs.

Received: 25 October 2013/ Revised version: 1 December 2013

DOI: 10.1007/s13320-013-0149-9
Article type: Regular

In the conventional system, the BGS is obtained by recording the probe wave power of one point at different frequencies directly. This means the power fluctuation of the microwave sweeper at different frequencies has been neglected, which may conduce the loss of the temperature accuracy and the strain accuracy [9].

In order to improve the accuracy of the BOTDA system, a novel method to eliminate the impact of microwave sweeper power fluctuation is proposed in this paper. In this scheme, comparing real-time acquisition of the probe wave power with a new algorithm, we can normalize the probe signals to eliminate this impact.

2. Theory

An M-Z EOM was employed in this system, and the structure diagram is shown in Fig. 1.

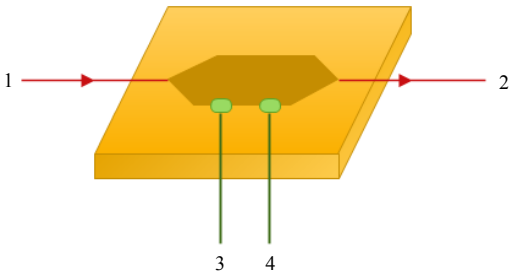

Fig. 1 Structure diagram of the EOM.

The CW wave was injected into the EOM through Port 1 with an electric field equation $E(t)=E_0\exp(j\omega_0 t)$ and then split into two branches via the first coupler in the EOM. Port 3 (bias voltage) and Port 4 (radio frequency voltage, RF voltage) were two electrical input ports of the EOM. One was for the direct current (DC) bias voltage, the other was for the microwave source RF voltage. Assuming the frequency of the microwave source is ω, the modulation voltage could be given by

$$V=V_{\mathrm{DC}}+V_m\cos(\omega t) \tag{1}$$

where V_{DC} and $V_m\cos(\omega t)$ are the DC bias voltage and microwave RF voltage, respectively. After the modulation, these two waves with the phase difference of φ join at the second coupler and transmit out of the EOM from Port 4. And the modulated wave could be described by (2):

$$E=E_0\exp(j\omega_0 t)\cos[C\cos(\omega t)+\varphi_{\mathrm{DC}}] \tag{2}$$

where C is modulation depth, and φ_{DC} is the phase change in V_{DC}. C can be calculated by $C=\pi V_m/(2V_\pi)$. The above equations show that the bias and RF voltages codetermine the working point of the EOM.

According to the Bessel function, (2) could be changed into

$$\begin{aligned}E=&E_0\cos(\omega_0 t)(J_0(C)+\\&2\sum_{n=1}^{\infty}[(-1)^n J_{2n}(C)\cos(2n\omega_m t)]\cos\varphi_{\mathrm{DC}}-\\&\{2\sum_{n=0}^{\infty}(-1)^n J_{2n+1}(C)\cos[(2n+1)\omega_m t]\sin\varphi_{\mathrm{DC}}\}\end{aligned} \tag{3}$$

where $J_n(C)$ is used to express the nth-order in the Bessel function [10]. From (3), it can be seen that the first-order modulated wave power with the frequency shift of ω is $\frac{1}{2}E_0^2J_1^2(C)[1-\cos(2\varphi_{\mathrm{DC}})]$.

In order to analyze the effect of the modulation depth on the modulation of the first order modulated wave, we measured the power of the first order modulated wave with different microwave power, as shown in Fig. 2.

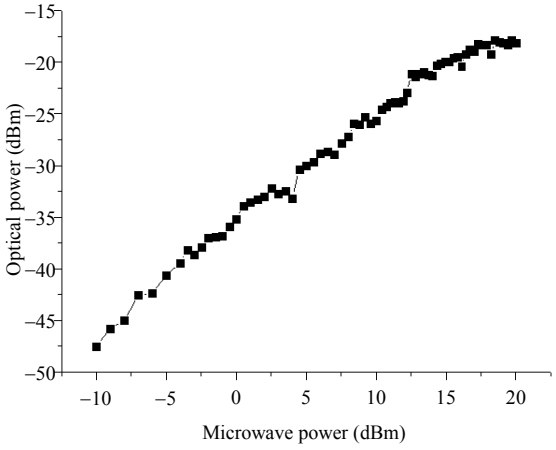

Fig. 2 Power of the first order modulated wave as a function of the microwave source power.

Figure 2 clearly indicates that the power of the first order modulated wave increases nearly linear

with the growing of the microwave source power. Setting the DC voltage to 7.3 V, then we employed the microwave sweeper to sweep the frequency at its maximum power. However, results showed that the intensity of the output wave from the EOM varied even with a totally certain incident intensity. Actually, it was derived from the power fluctuation of the microwave sweeper. The power of the microwave sweeper was fluctuated from 17.5 dBm to 20 dBm when it swept from 10000 MHz to 12000 MHz. The power change in the output modulated wave has been experimented and listed in Fig. 3.

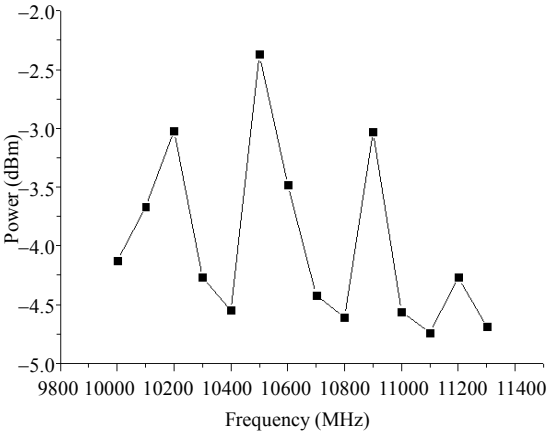

Fig. 3 Power of the modulated wave as a function of the frequency of the microwave source.

From this figure, we can notice that the modulated CW wave also has about 2.5 dB of fluctuation. In the BOTDA system, the probe wave we detected can be expressed as a function of the first order modulated wave I_{CW}:

$$I_{\mathrm{CW}}(t,\Delta\nu) = I_{\mathrm{CW}}\exp(-\alpha L)\times \exp[\int_{\frac{v_g t}{2}}^{\frac{v_g t}{2}+\Delta z} g_B(\xi,\Delta\nu) I_P(\xi,\Delta\nu) d\xi] \quad (4)$$

where I_{CW} is the input CW probe wave intensity at the far end of the fiber $z = L$, α is the fiber loss, L is the fiber length, υ_g is the group velocity, Δz is the spatial resolution related to the pump pulse duration, $\Delta\nu$ is the frequency offset between the two counter-propagating optical signals, and $g_B(\xi,\Delta\nu)$ and $I_P(\xi,\Delta\nu)$ are the BGS and the pump intensity at position $z = \xi$. Equation (4) points out that the detected probe wave strongly depends on the I_{CW} [11]. Therefore, the maximum peak power in the SBS gain spectrum we obtained by the conventional method may not correspond to the Brillouin frequency shift. That is why the power fluctuation of the microwave sweeper should not be neglected.

In order to cover the shortage in the conventional measuring method and improve the accuracy of measurement, a novel method to eliminate the impact of microwave sweeper power fluctuation is proposed in this paper. For simplification, assuming that

$$f(t,\Delta\nu) = \exp(-\alpha L)\exp[\int_{\frac{v_g t}{2}}^{\frac{v_g t}{2}+\Delta z} g_B(\xi,\Delta\nu) I_P(\xi,\Delta\nu) d\xi],$$

then (4) could turn into

$$I_{\mathrm{CW}}(t,\Delta\nu) = I_{\mathrm{CW}} \times f(t,\Delta\nu). \quad (5)$$

In the ideal situation, I_{CW} has the same scale in different frequencies, so that $I_{\mathrm{CW}}(t,\Delta\nu)$ can reflect the Brillouin frequency shift distribution directly. But that is not the case when $I_{\mathrm{CW}}(t,\Delta\nu)$ is unstable. In consideration of eliminating fluctuation impact of I_{CW}, (5) turns into

$$\frac{I_{\mathrm{CW}}(t,\Delta\nu)}{I_{\mathrm{CW}}} = f(t,\Delta\nu). \quad (6)$$

In this case, $I_{\mathrm{CW}}(t,\Delta\nu)/I_{\mathrm{CW}}$ depends just on the frequency, which means we can obtain the real Brillouin gain spectrum as long as we calculate the value of $I_{\mathrm{CW}}(t,\Delta\nu)/I_{\mathrm{CW}}$.

The round-trip time in the 1-km optical fiber for the Brillouin signal was 10 μs. In our experiment, we chose a pulse wave with a period longer than the duration of Brillouin energy transfer in per period. The probe wave intensity without Brillouin energy transfer can be expressed as $I_{\mathrm{CW}}\exp(-\alpha L)$. By calculating the average value of the signal intensity at this segment, I_{CW} could be obtained. Gauss fit is applied in the BGS to express our experimental result more clearly.

3. Experiment

3.1 Experimental setup

The experimental scheme is depicted in Fig. 4. A laser diode (LD) operating at 1550 nm with the 1.9-MHz linewidth and 15-dBm power was used. The linewidth of the laser has impact on the measurement accuracy. In our system, 1.08-MHz variation in the Brillouin frequency shift corresponds to 1- ℃ variation in temperature. Therefore, the laser with the 1.9-MHz linewidth would lead to the temperature error within 1.76 ℃. Then, a 1:1 optical coupler was used to split the laser into pump and probe waves. The probe wave was intensity-modulated by an EOM with the 10-GHz bandwidth driven by the microwave sweeper to create two sidebands. After setting the proper bias voltage and the polarization controller, the up-shifted sideband was suppressed by the filter constituted by a circulator and a 0.1-nm bandwidth fiber Bragg grating (FBG). Then, the –10-dBm probe wave was injected into the sensing fiber. In the other branch, the pump wave was modulated into pulse by an AOM with the 200-MHz bandwidth and more than 50-dB extinction ratio and amplified by the erbium doped fiber amplifier (EDFA). A polarization-scrambler (PS) was used to suppress the polarization-dependent gain fluctuation [12]. The pump with about 20-dBm power, 80-ns pulse width, and 10-kHz repetition frequency was injected into the other end of the sensing fiber. Our probe signals were recorded at 150 MHz using 2000 average.

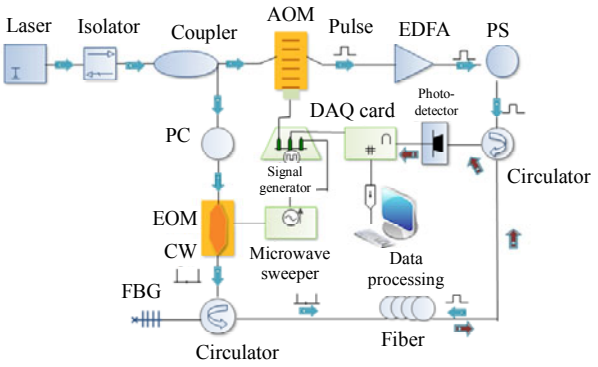

Fig. 4 Experimental setup of the BOTDA system.

3.2 Experimental process

To validate the benefit of the novel method, the contrast experiment between the conventional and new methods was carried out. The test section was the 130-m segment of the optical fiber located from 4000 m – 4130 m, which was placed into the thermostat to be heated to different temperatures.

We measured the frequency values at the point of the maximum Brillouin gain at 30 ℃, 45 ℃, 60 ℃, and 75 ℃, respectively by using the conventional and new methods. Figure 5 shows the temperature changes during the range of 4000 m to 4130 m.

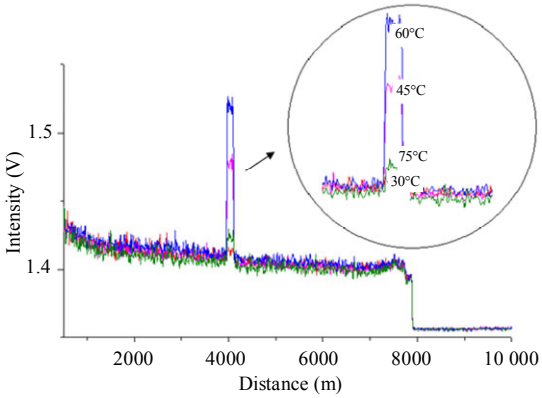

Fig. 5 Collected probe wave curves at different temperature.

The recorder Gauss fit of the BGS at one point of the test section by the conventional method was figured out and shown in Fig. 6(a). When using the new method to eliminate the impact of microwave sweeper power fluctuation, the BGS can be completely measured, and the whole probe wave is described by a fitting Gauss curve, as shown in Fig. 6(b).

Obviously, the widths of the BGS shown in Figs. 6(a) and 6(b) are quite different. This is attributed to the irregular power fluctuations of the microwave sweeper, which gives rise to some undesired effects upon both direct component and alternating component and then conduces distortion of the BGS in Fig. 6(a).

The before-and-after temperature measurement results are shown in Table 1.

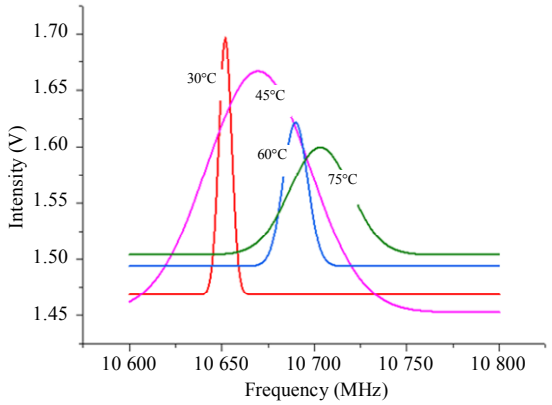

(a) In the conventional method

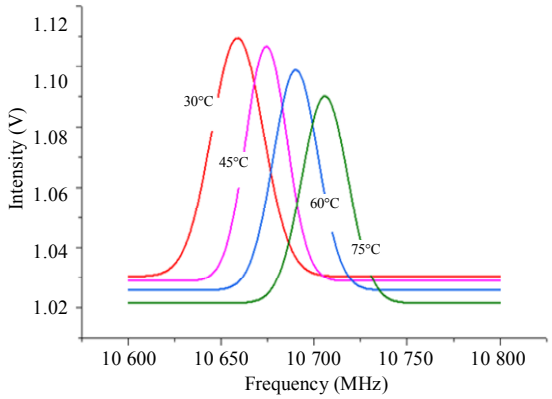

(b) In the new method

Fig. 6 Fitting results of BGS at different temperatures.

Table 1 Temperature accuracy contrast.

Actual temperature (℃)	In the conventional method (℃)	In the new method (℃)
30	25.36	30.64
45	40.55	44.73
60	58.91	59.09
75	71.09	73.36

In the conventional method, the temperature accuracy was about ±5 ℃. And the temperature accuracy in the proposed method became ±2 ℃, which was improved about 3 ℃. It can be seen that the errors obtained by the new method were smaller than that in the conventional one. Thus, the accuracy was improved clearly visible when using our new method.

4. Conclusions

In conclusion, we performed a theoretical analysis and experimental implementation for eliminating the impact of microwave sweeper power fluctuation in the BOTDA system. By comparing real-time acquisition of the probe wave power with a new algorithm to normalize the optical signal, the measurement error caused by the probe wave fluctuation can be eliminated. Experimental results showed that the impact of microwave sweeper power fluctuation in the BOTDA system was eliminated, and the temperature accuracy was improved 2.5 times to ±2 ℃ effectively compared to the conventional method. And it is demonstrated that this method can be very efficient, and it is of great potential for achieving high signal to noise ratio (SNR) in the BOTDA systems.

Acknowledgement

This work was supported by Natural Science Foundation of China (60977058), Independent Innovation Foundation of Shandong University (IIFSDU2010JC002 & 2012JC015), and the key technology projects of Shandong Province (2010GGX10137).

Reference

[1] X. P. Zhang, Y. G. LU, F. Wang, H. Liang, and Y. X. Zhang, "Development of fully-distributed fiber sensors based on Brillouin scattering," *Photonic Sensors*, 2011, 1(1): 54–61.

[2] W. J. Wang, J. Chang, G. P. Lv, Z. L. Wang, Z. Liu, S. Luo, *et al.*, "Wavelength dispersion analysis on fiber-optic Raman distributed temperature sensor system," *Photonic Sensors*, 2013, 3(3): 256–261.

[3] Y. K. Dong, L. Chen, and X. Y. Bao, "Time-division multiplexing-based BOTDA over 100 km sensing length," *Optics Letters*, 2011, 36(2): 277–279.

[4] S. R. Cui, S. Pamukcu, A. X. Lin, W. Xiao, D. Herr, J. Toulouse, and M. Pervizpour, "Distributed temperature sensing system based on Rayleigh scattering BOTDA," *IEEE Sensors Journal*, 2011, 11(2): 399–403.

[5] W. R. Habel and K. Krebber, "Fiber-optic sensor applications in civil and geotechnical engineering," *Photonic Sensors*, 2011, 1(3): 268–280.

[6] Y. Peled, A. Motil, L. Yaron, and M. Tur, "Slope-assisted fast distributed sensing in optical fibers with arbitrary Brillouin profile," *Optics Express*, 2011, 19(21): 19845–19865.

[7] J. Urricelqui, A. Zornoza, M. Sagues, and A. Loayssa, "Dynamic BOTDA measurements based on Brillouin phase-shift and RF demodulation," *Optics Express*, 2012, 20(24): 26942–26949.

[8] X. H. Jia, Y. J. Rao, K. Deng, Z. X. Yang, L. Chang, C. Zhang, *et al.*, "Experimental demonstration on 2.5-m spatial resolution and 1 ℃ temperature uncertainty over long-distance BOTDA with combined Raman amplification and optical pulse coding," *IEEE Photonics Technology*, 2011, 23(7): 435–437.

[9] J. B. Wang, Y. G. Lu, X. P. Zhang, and F. Wang, "Calibration of reference light power in Brillouin optical time domain reflectometer," *Chinese Journal of Lasers*, 2010, 37(6): 1456–1461.

[10] H. J. Zhou, Z. Meng, and Y. Liao, "Frequency shift characteristics analysis of $LiNbO_3$ waveguide electro-opticIntensity," *Chinese Journal of Lasers*, 2009, 36(4): 901–905.

[11] C. Bao, M. P. Song, and X. F. Ye, "Polarization control techniques in the Brillouin optical time domain analyzer," *Chinese Journal of Sensors and Actuators*, 2010, 23(2): 201–204.

[12] M. A. Soto, G. Bolognini, and F. D. Pasquale, "Analysis of pulse modulation format in coded BOTDA sensors," *Optics Express*, 2010, 18(14): 14878–14892.